IOPscience iopscience.iop.org

Home Search Collections Journals About Contact us My IOPscience

Jitter-correction for IR/UV-XUV pump-probe experiments at the FLASH free-electron laser

This content has been downloaded from IOPscience. Please scroll down to see the full text.

2017 New J. Phys. 19 043009

(http://iopscience.iop.org/1367-2630/19/4/043009)

View the table of contents for this issue, or go to the journal homepage for more

Download details:

IP Address: 129.130.38.152
This content was downloaded on 10/08/2017 at 19:59

Please note that terms and conditions apply.

You may also be interested in:

Time-diagnostics for improved dynamics experiments at XUV FELs
Markus Drescher, Ulrike Frühling, Maria Krikunova et al.

Compact XFEL and AMO sciences: SACLA and SCSS
M Yabashi, H Tanaka, T Tanaka et al.

Femtosecond x-ray photoelectron diffraction on gas-phase dibromobenzene molecules
D Rolles, R Boll, M Adolph et al.

Towards imaging of ultrafast molecular dynamics using FELs
A Rouzée, P Johnsson, L Rading et al.

Coulomb explosion of diatomic molecules in intense XUV fields mapped by partial covariance
O Kornilov, M Eckstein, M Rosenblatt et al.

Ultra-fast and ultra-intense x-ray sciences: first results from the Linac Coherent Light Source free-electron laser
C Bostedt, J D Bozek, P H Bucksbaum et al.

Strongly aligned gas-phase molecules at free-electron lasers
Thomas Kierspel, Joss Wiese, Terry Mullins et al.

Field-free molecular alignment probed by FLASH
P Johnsson, A Rouzée, W Siu et al.

Time-resolved ion spectrometry on xenon with jitter-compensated soft-x-ray pulses of a free-electron laser
Maria Krikunova, Theophilos Maltezopoulos, Armin Azima et al.

New Journal of Physics
The open access journal at the forefront of physics

Deutsche Physikalische Gesellschaft DPG
IOP Institute of Physics

Published in partnership with: Deutsche Physikalische Gesellschaft and the Institute of Physics

OPEN ACCESS

RECEIVED
21 December 2016

REVISED
6 February 2017

ACCEPTED FOR PUBLICATION
7 March 2017

PUBLISHED
10 April 2017

Original content from this work may be used under the terms of the Creative Commons Attribution 3.0 licence.

Any further distribution of this work must maintain attribution to the author(s) and the title of the work, journal citation and DOI.

PAPER

Jitter-correction for IR/UV-XUV pump-probe experiments at the FLASH free-electron laser

Evgeny Savelyev[1], Rebecca Boll[1], Cédric Bomme[1], Nora Schirmel[1], Harald Redlin[1], Benjamin Erk[1], Stefan Düsterer[1], Erland Müller[1], Hauke Höppner[1,2], Sven Toleikis[1], Jost Müller[1], Marie Kristin Czwalinna[1], Rolf Treusch[1], Thomas Kierspel[3,4], Terence Mullins[3], Sebastian Trippel[3,4], Joss Wiese[3], Jochen Küpper[3,4,5], Felix Brauβe[6], Faruk Krecinic[6], Arnaud Rouzée[6], Piotr Rudawski[7], Per Johnsson[7], Kasra Amini[8], Alexandra Lauer[8], Michael Burt[8], Mark Brouard[8], Lauge Christensen[9], Jan Thøgersen[9], Henrik Stapelfeldt[9], Nora Berrah[10], Maria Müller[11], Anatoli Ulmer[11], Simone Techert[1,12,13], Artem Rudenko[14] and Daniel Rolles[1,14,15]

[1] Deutsches Elektronen-Synchrotron DESY, D-22607 Hamburg, Germany
[2] Institut für Physik, Carl von Ossietzky Universität, D-26111 Oldenburg, Germany
[3] Center for Free-Electron Laser Science (CFEL), Deutsches Elektronen-Synchrotron DESY, D-22607 Hamburg, Germany
[4] Center for Ultrafast Imaging, Universität Hamburg, D-22761 Hamburg, Germany
[5] Department of Physics, Universität Hamburg, D-22761 Hamburg, Germany
[6] Max-Born-Institut für nichtlineare Optik und Kurzzeitspektroskopie, D-12489 Berlin, Germany
[7] Department of Physics, Lund University, SE-22100 Lund, Sweden
[8] The Chemistry Research Laboratory, Department of Chemistry, University of Oxford, Oxford OX1 3TA, United Kingdom
[9] Department of Chemistry, Aarhus University, DK-8000 Aarhus C, Denmark
[10] Department of Physics, University of Connecticut, Storrs, CT 06269, United States of America
[11] Institut für Optik und atomare Physik, Technische Universität Berlin, D-10623 Berlin, Germany
[12] Max Planck Institute for Biophysical Chemistry, D-33077 Göttingen, Germany
[13] Institute for x-ray Physics, Göttingen University, D-33077 Göttingen, Germany
[14] J.R. Macdonald Laboratory, Department of Physics, Kansas State University, Manhattan, KS 66506, United States of America
[15] Author to whom any correspondence should be addressed.

E-mail: rolles@phys.ksu.edu

Keywords: free-electron laser, pump-probe experiments, photodissociation, velocity map imaging, time-resolved ion imaging

Abstract

In pump-probe experiments employing a free-electron laser (FEL) in combination with a synchronized optical femtosecond laser, the arrival-time jitter between the FEL pulse and the optical laser pulse often severely limits the temporal resolution that can be achieved. Here, we present a pump-probe experiment on the UV-induced dissociation of 2,6-difluoroiodobenzene ($C_6H_3F_2I$) molecules performed at the FLASH FEL that takes advantage of recent upgrades of the FLASH timing and synchronization system to obtain high-quality data that are not limited by the FEL arrival-time jitter. We discuss in detail the necessary data analysis steps and describe the origin of the time-dependent effects in the yields and kinetic energies of the fragment ions that we observe in the experiment.

1. Introduction

Free-electron lasers (FELs) (Ackermann *et al* 2007, Shintake *et al* 2008, Emma *et al* 2010, Allaria *et al* 2012, Ishikawa *et al* 2012) deliver intense, extreme ultraviolet (XUV) and x-ray pulses with pulse lengths ranging from a few to a few hundred femtoseconds, thus providing unprecedented opportunities for ultrafast time-resolved experiments in the XUV to x-ray regime. Such pump-probe experiments allow ultrafast processes to be studied in a variety of samples, including atoms and molecules (Meyer *et al* 2006, Radcliffe *et al* 2007, Meyer *et al* 2008, Johnsson *et al* 2009, Krikunova *et al* 2009, Glownia *et al* 2010, Meyer *et al* 2010, Jiang *et al* 2010a, 2010b, 2010c, Krikunova *et al* 2011, Petrovic *et al* 2012, Düsterer *et al* 2013, Jiang *et al* 2013, Rouzée *et al* 2013, Schnorr *et al* 2013, Boll *et al* 2014, Erk *et al* 2014, Fang *et al* 2014, McFarland *et al* 2014, Rolles *et al* 2014, Schnorr *et al* 2014a, 2014b, Liekhus-Schmaltz 2015, Minitti *et al* 2015, Rudenko and Rolles 2015, Schnorr *et al* 2015, Boll

© 2017 IOP Publishing Ltd and Deutsche Physikalische Gesellschaft

et al 2016, Budarz et al 2016, Lehmann et al 2016, Picon et al 2016), clusters and nanoparticles (Krikunova et al 2012a, 2012b, Clark et al 2015, Ferguson et al 2016, Flückiger et al 2016, Gorkhover et al 2016), liquids (Hallmann et al 2010, Wernet et al 2015, Biasin et al 2016), solids (Rajkovic et al 2010, Dell'Angela et al 2013, Siefermann et al 2014, Gleason et al 2015, Öström et al 2015, Rettig et al 2016), and even biological systems such as photoactive proteins (Aquila et al 2012, Tenboer et al 2014, Barends et al 2015, Pande et al 2016). Many of these time-resolved experiments require precise synchronization of an optical femtosecond laser with the FEL. Early synchronization and locking schemes mostly relied on electronic radio-frequency (RF) synchronization (Glownia et al 2010, Redlin et al 2011), where long-term drifts and shot-to-shot jitter of the arrival time of the FEL pulse significantly limited the temporal resolution far beyond the pulse durations of the FEL and the femtosecond laser (Radcliffe et al 2007, Glownia et al 2010, Petrovic et al 2012, Rouzée et al 2013, Rolles et al 2014, Schnorr et al 2014b). To address these limitations, x-ray/optical cross-correlators (OXCs) were developed, which measure the relative arrival-time jitter between the FEL and laser pulses on a shot-by-shot basis to offer the ability to correct for this jitter by sorting the data through post-analysis (Gahl et al 2008, Maltezopoulos et al 2008, Azima et al 2009, Drescher et al 2010, Bionta et al 2011, Beye et al 2012, Grguraš et al 2012, Schorb et al 2012, Harmand et al 2013, Riedel et al 2013, Bionta et al 2014, Eckert et al 2015). While such cross-correlation schemes significantly improved the temporal resolution that could be achieved in pump-probe experiments, the method is applicable only to certain types of experiments. One of the most significant limitations is in the transport of the FEL pulses into the cross-correlator, requiring either the cross-correlator or the experiment to be transparent, depending on whether the cross-correlator is placed in front of or behind the experiment. Furthermore, if the FEL beam is very divergent, for example, when using focusing mirrors with a short focal length, the minimum fluence required for such cross-correlation measurements makes it necessary to refocus the FEL beam into the cross-correlation setup. These requirements impose many technical and geometric constraints and, in some cases, make it impossible to use a cross-correlation scheme for the pump-probe experiment.

In order to develop a generally applicable solution, the FEL in Hamburg (FLASH) pursued an alternative, additional strategy. First, an optical synchronization system based on stabilized optical links (Kim 2007) was implemented, which allowed the development of a bunch arrival-time monitor (BAM) that uses the electron bunch for a cross-correlation with a synchronized optical reference (Löhl et al 2010). Subsequently, the pump-probe laser synchronization was upgraded from a pure electronic RF-based system to an all-optical synchronization that includes several timing stabilization schemes (Schulz et al 2015). These modifications were expected to dramatically improve the stability and temporal resolution of pump-probe experiments that combine the FLASH XUV beam with the FLASH pump-probe laser, which may ultimately remedy the need for an additional x-ray/optical arrival-time measurement.

Here, we demonstrate how the increased timing stability and shot-by-shot sorting according to the bunch arrival-time data can dramatically improve the quality of pump-probe data, shown exemplarily for the case of photo-induced dissociation of gas-phase 2,6-difluoroiodobenzene. A description of the experimental setup is presented in section 2, followed by the experimental results with a detailed description of the data sorting and analysis scheme in section 3, which illustrates how the individual steps of this scheme affect and improve the data.

2. Experimental setup

The experiment described here was performed on the focused branch of beamline BL3 at the FLASH FEL (Feldhaus 2010) at DESY in Hamburg, Germany. It used a pulsed molecular beam for sample delivery, a near-infrared (NIR) laser for adiabatically laser-aligning the molecules in the laboratory frame, a UV laser for dissociating the molecules (the 'pump' process), and the XUV-FEL to probe the dissociating molecules. A more detailed description of the experimental approach and the technical parameters of the pump-probe experiment is given in section 2.1, followed by a short description of the FLASH timing and diagnostics system in section 2.2.

2.1. Setup of the pump-probe experiment

At FLASH, an electron bunch produced by irradiating a photocathode with a picosecond laser is accelerated to relativistic energies in a superconducting linear accelerator. It then passes through a long magnetic undulator, where an intense, femtosecond XUV pulse is produced via self-amplified spontaneous emission (SASE) (Ackermann et al 2007). For the experiments described here, FLASH was operated at 0.6 GeV electron energy in single-bunch mode (i.e. 10 Hz repetition rate) with 180 pC bunch charge, producing XUV pulses at a central wavelength of 11.5 nm (107.8 eV photon energy, bandwidth (FWHM): 2 eV) with an average pulse energy of 37 μJ. From the measurement of the electron bunch duration performed several times during each FEL shift, the pulse duration of the XUV pulses was estimated to be approximately 50 fs (rms), corresponding to 120 fs

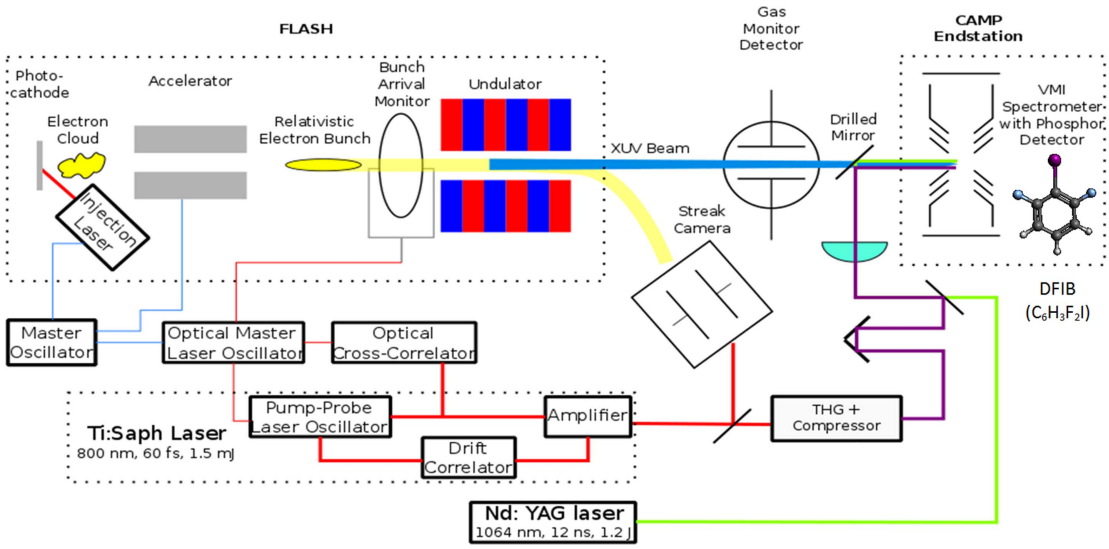

Figure 1. Sketch of the experimental setup for the pump-probe experiment at FLASH, as described in detail in the text, including some of the elements of the FLASH timing, synchronization, and diagnostics system that are of particular importance to the data analysis. The thick red, green, and purple lines are 800 nm, 1064 nm, and 267 nm laser beams, the thin red lines are length-stabilized optical fiber links (Kim 2007), and the thin blue lines are electronic (RF) timing connections.

(FWHM), assuming a factor of 0.5 between the electron bunch and photon pulse duration. For further details on how the electron bunch duration is measured and how the photon pulse duration is estimated from this, see (Behrens *et al* 2012, Düsterer *et al* 2014). After the undulator, the XUV pulse was transported to the experimental station by a series of carbon-coated grazing-incidence mirrors and focused to a spot size of ~20 μm (FWHM) using an ellipsoidal mirror (Feldhaus 2010). At the interaction region inside the CAMP end-station (Strüder *et al* 2010), the focused XUV beam was intersected with a cold molecular beam of 2,6-difluoroiodobenzene ($C_6H_3F_2I$, 'DFIB', see inset in figure 1) molecules, seeded in neon carrier gas, that was produced by supersonic expansion through a pulsed Even-Lavie valve (nozzle size: 100 μm, valve opening time: 12.5 μs) operated at 70 °C and with a 20 bar backing pressure of the carrier gas. The molecular beam expansion chamber was separated from the main chamber by two skimmers (*Beam Dynamics* model 50.8, skimmer sizes 2 and 4 mm), with an electrostatic deflector (Filsinger *et al* 2009, Küpper *et al* 2014, Stern *et al* 2014), operated at ±11 kV, installed in between the two skimmers. The deflector was used in order to separate the DFIB molecules from the carrier gas and to select molecules in the lowest rotational quantum states, which increases the degree of molecular alignment that can be achieved (Holmegaard *et al* 2009, Nevo *et al* 2009).

The molecular beam was also intersected by UV and NIR laser pulses that were focused to an estimated spot size of 50 μm (FWHM) by an out-of-vacuum focusing lens (focal length $\approx$ 60 cm) and overlapped (near-) collinearly with the XUV beam, as sketched in figure 1, using a 2' drilled mirror (*Eksma Optics*) with a conical hole (2 mm diameter on coated side) that was high-reflectivity coated for 267, 800, and 1064 nm. The focal lengths for the three colors were adjusted by adjusting the divergence of the laser beams with lens telescopes.

The elliptically polarized NIR pulses (wavelength: 1064 nm, pulse duration: 12 ns, pulse energy: 1.2 J) were generated by an injection-seeded Nd:YAG laser (*Spectra Physics* Quanta Ray Pro 270-50) that was electronically synchronized to the FLASH bunch trigger. They were used to adiabatically three-dimensionally align (Larsen *et al* 2000, Stapelfeldt and Seideman 2003, Nevo *et al* 2009) the DFIB molecules. The molecules were aligned with their most polarizable molecular axis, i.e. the axis along the carbon–iodine bond, along the major polarization axis of the Nd:YAG laser pulses, which was parallel to the polarization direction of the XUV pulses and also parallel to the detector plane, and with the plane of the phenyl ring perpendicular to the propagation direction of the laser beams. The relative timing between the XUV and the Nd:YAG pulses was adjusted such that the maximum alignment, which occurs at the maximum of the laser field, is reached upon arrival of the XUV pulse.

The UV pulses (center wavelength 267 nm, bandwidth: 2.5 nm FWHM) were generated by frequency tripling the FLASH 10 Hz Ti:Sapphire pump-probe laser (Redlin *et al* 2011) in the FLASH in-house third-harmonic generation setup, and were compressed to an estimated (150 +/− 50) fs (FWHM) pulse duration on target using a prism compressor. We note that the bandwidth, which was measured directly at the output of the third harmonic generation unit, is sufficient to support significant shorter pulse durations, but under the given experimental conditions, we were not able to compress them to their Fourier transform limit. The pulse energy of the UV pulses before entering the vacuum chamber was 35 μJ and the polarization direction was parallel to the XUV pulses. The relative timing between the UV-pump and the XUV-probe pulses was controlled by a

motorized delay stage and was typically varied between +1 ps (corresponding to the XUV-probe pulse arriving 1 ps *after* the UV-pump pulse) and −1 ps (corresponding to the XUV-probe pulse arriving 1 ps *before* the UV-pump pulse). When the UV-pump pulse arrived before the XUV pulse, the aligned DFIB molecules were first photodissociated by the UV pulse and the XUV pulse subsequently probed the molecules while they were undergoing the photodissociation reaction. When the UV pulse arrived after the XUV pulse, only intact, aligned DFIB molecules were probed by the XUV pulse.

The momentum distribution of the electrons and ions produced by the interaction between the XUV pulses and the molecules were imaged using a double-sided velocity map imaging (VMI) spectrometer (Strüder *et al* 2010, Rolles *et al* 2014) equipped with two 80 mm MCP-phosphor screen detectors (*Photonis* APD 2 PS 75/32/25/8 I 60:1). The high voltage for both detectors was rapidly switched on and off using fast high-voltage push-pull switches (*Behlke* HTS 31-03-GSM) in order to discriminate photo- and Auger electrons from stray light and secondary electrons, as well as to selectively record the ion VMI image for one specific ionic species. For the electrons, a P20 phosphor screen was used, while the ion-side of the spectrometer was equipped with a fast P47 phosphor screen. Both electron and ion images were recorded at 10 Hz using commercial high-speed CCD cameras (*Allied Vision* Pike F-145B).

In order to analyze the resulting pump-probe delay-dependent electron and ion images, it is essential to (i) normalize the data to the fluctuating XUV pulse energy and (ii) to correct for the arrival-time jitter between the XUV and the UV pulses using the FLASH timing and diagnostics system that is briefly described in the following section. The normalization and jitter-correction steps and their effects on the pump-probe data are described in detail in section 3.

2.2. The FLASH diagnostics, timing and synchronization system

The FLASH diagnostics system is designed to measure as many parameters of the XUV and laser pulses as possible on a shot-to-shot, non-invasive basis. It runs in parallel with the user experiment and records these parameters along with a unique 32 bit pulse ID in the FLASH data acquisition (DAQ) data stream. The experimental data can then be sorted and corrected based on this machine data in the post-analysis. For example, the XUV pulse energy (and the FEL beam position) is measured for each FEL shot using the gas monitor detector (GMD) (Tiedtke *et al* 2008). In the GMD, which is installed behind the SASE undulators at the upstream entrance to the FLASH experimental hall, as sketched in figure 1, the XUV beam passes through an ionization chamber filled with a noble gas (here, krypton at a pressure of $\sim 1.6 \times 10^{-6}$ mbar). The gas pressure in the GMD is low enough to transmit more than 99% of the XUV photons, but sufficient photoelectrons and ions are created such that the current, collected in two Faraday cups, can be converted into XUV pulse energy.

The overall timing of the FLASH accelerator is controlled by the FLASH master oscillator (MO), to which the injector laser, the accelerator, and the optical master laser oscillator (MLO) are connected via electronic RF connections (see figure 1). The Ti:Sapphire pump-probe laser is actively stabilized to the MLO with an all-optical feedback and stabilization system (Schulz *et al* 2015). It includes a balanced OXC, which stabilizes the output of the pump-probe laser's oscillator to the MLO via a 10 kHz fast feedback system, and an additional cross-correlator ('drift correlator') to correct for slow drifts of the laser amplifier stage with respect to the oscillator stage via a slow 1 Hz feedback loop. When the active stabilization is enabled, a synchronization of the pump-probe laser to the optical reference to below 10 fs (rms) is possible (Schulz *et al* 2015).

However, for measurements that employ both the FLASH pump-probe laser and the FEL, there is an additional jitter that contributes significantly to the overall temporal resolution. This jitter stems from shot-to-shot variations in the electron bunch arrival time, which mainly results from fluctuations of the electron bunch energy and thus varying flight times through the bunch compressor chicanes in the accelerator. In order to measure this arrival-time jitter between the MLO and the electron bunch in the accelerator, which is typically on the order of 100 fs (rms), several BAMs are installed in the FLASH accelerator (Czwalinna 2012). In the BAMs, a RF pickup with several 10 GHz bandwidth couples the electrical transient signal from the passing electron bunch into a coaxial line that is connected to an electro-optical modulator. From the amplitude of the modulated laser pulse, the relative arrival time with respect to the MLO can be determined, which is then recorded in the FLASH DAQ on a shot-to-shot basis. Depending on the FEL beam parameters, in particular the electron bunch charge, the resolution of the BAMs can reach 5 fs (Czwalinna 2012). For the present measurement, which was performed at a relatively low bunch charge of 180 pC in order to generate short XUV pulses, the resolution of the BAMs was approximately 15 fs. The signal from the BAM can also be used in an active-feedback loop to stabilize the timing of the electron bunches with respect to the MLO. When the 'slow (1 Hz) feedback' is enabled and properly functioning, this stabilizes the overall arrival time and thus reduces drifts but does *not* reduce the shot-to-shot jitter. An additional 'fast (intra-pulse-train) feedback' can also reduce the shot-to-shot jitter between bunches within one bunch train, but this fast feedback is currently not applicable for 10 Hz 'single-bunch' operation, which is used for the majority of pump-probe experiments involving the optical laser at FLASH.

The BAMs inherently only measure relative timing changes between the electron bunches and the synchronized optical reference, with a dynamic range limited to 4 ps. For larger drifts or jumps in the electron bunch timing, a motorized optical delay line inside the BAM is automatically adjusted in order to stay inside the measurement window. However, the RF signal from the MO which is used to accelerate the electron bunches is not yet synchronized to the optical MLO. Therefore, phase drifts of the distributed RF signals lead to long-term drifts of the overall, absolute electron bunch timing. Since this effect, as well as other long-term drifts due to thermal fluctuations that lead to length variations in the beamlines, cannot be recorded by the BAMs, these long-term drifts in the relative timing between the electron bunch in the accelerator and the pump-probe laser pulses are, in addition, measured by a streak camera (Redlin *et al* 2011), which has a working range of 80 ps. The streak camera monitors the relative timing between the output of the pump-probe laser and the dipole radiation generated by the electron bunch in the bending magnet that splits the trajectories of the photon and electron beams and directs the latter into the electron beam dump. The streak camera measurement occurs every two seconds and is saved locally on a computer. In order to achieve sub-picosecond resolution, a running average over the last 20 data points is calculated automatically and this averaged value is saved to the FLASH DAQ. The temporal resolution of the average is typically around 200 fs (rms), and since it is not a single-shot measurement, it cannot be used to correct the shot-to-shot arrival-time jitter. However, the streak camera is the only diagnostic that measures directly the output of the pump-probe laser against the FEL electron bunch, while all other timing measurements are with respect to a common reference provided by the MO.

3. Results and discussions

In this section, the experimental results and their subsequent improvement upon sorting and normalization on the FLASH machine data are presented. We first discuss the general interpretation of the pump-probe data in section 3.1, before describing the detailed data analysis steps in section 3.2.

3.1. UV-induced photodissociation and XUV multi-photon inner-shell ionization of 2,6-difluoroiodobenzene

In addition to developing and testing a procedure for jitter correction in FEL-based UV-pump XUV-probe experiments, a further goal of our study is the investigation of the UV-induced photodissociation of 2,6-difluoroiodobenzene (DFIB) molecules in the gas phase. DFIB (both the 2,6- and the 3,5-isomers) has been used as a target molecule in several laser-induced molecular alignment experiments (Viftrup *et al* 2007, Nevo *et al* 2009, Ren *et al* 2014). In a recent study, the dissociation of 3,5- and 2,4-DFIB at various UV-wavelengths and the formation of neutral and excited atomic iodine fragments was investigated by a combined experimental and theoretical approach that enabled the determination of dissociation energies, the total kinetic energy release, fragment ion anisotropy parameters, and a discussion of the electronic states involved in the dissociation process (Murdock *et al* 2012). In the experiment described here, we investigated the UV-induced dissociation of 2,6-DFIB and, in particular, the charge transfer process that occurs after inner-shell ionization using time-resolved photoelectron and ion imaging. For this purpose, the DFIB molecules in the molecular beam were first irradiated with a femtosecond UV (267 nm) pulse and the induced photoreaction was then probed, at various time delays, by an intense, femtosecond XUV (11.5 nm/107.8 eV photon energy) pulse from the FLASH FEL. At this XUV photon energy, which is approximately 50 eV above the iodine 4d ionization threshold in 2,6-difluoroiodobenzene (DFIB), the partial photoionization cross-section of the iodine 4d shell is around 3.8 Mb (Yeh 1993). Emission of an I(4d) inner-shell photoelectron is typically followed by rapid Auger decay into doubly or triply charged cationic states (Ablikim *et al* 2017), which generally fragment into two or more charged fragments that are emitted with relatively high kinetic energies due to the Coulomb repulsion of the positive charges (hence, this process is also referred to as 'Coulomb explosion'). Alternatively, absorption of an XUV photon can also lead to the emission of an electron from the molecular valence shell, which predominantly leads to singly charged bound or dissociating final states. Within the intense XUV pulses produced by FLASH, a single DFIB molecule can absorb more than one XUV photon, and the molecules thus typically fragment into several singly and multiply charged fragments. The double-sided VMI spectrometer used in this experiment allows the measurement of the kinetic energies and angular distributions of photoelectrons and Auger electrons as well as the fragment ions that are created in this multi-photon ionization process. In the following, we will concentrate on discussing the fragment ion measurements, while the electron measurements will be discussed in a separate publication.

Figure 2 shows the ion images and corresponding kinetic energy spectra of I^{3+} ions measured with the VMI spectrometer for different delays between the UV and the XUV pulses. As we explain in the following, their kinetic energy can be used to obtain information about the distance between the iodine atom and the rest of the molecule at the time when the charge was created. The UV pulse alone does not create any I^{3+} ions at the

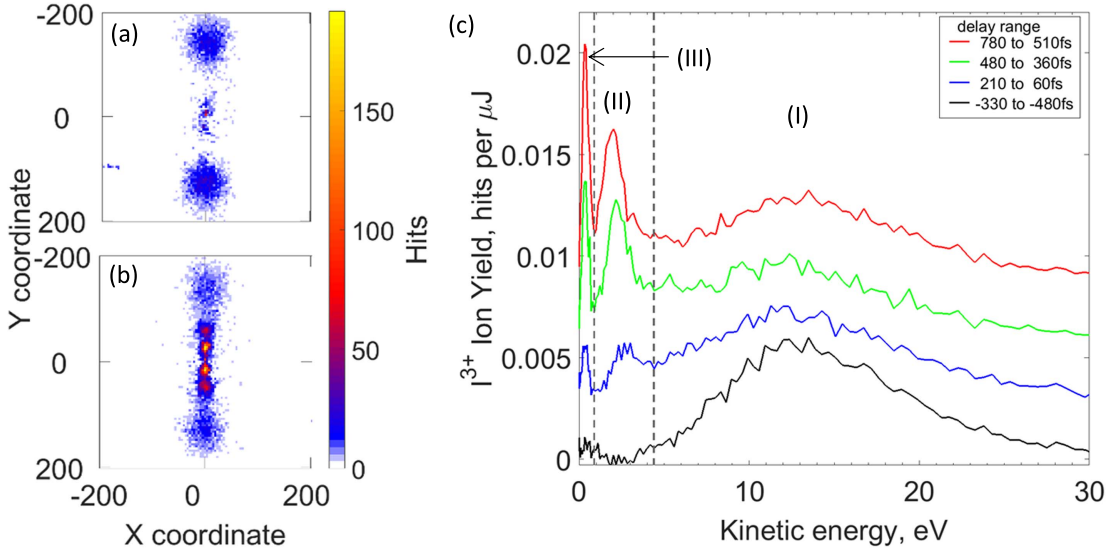

Figure 2. Ion images (i.e. two-dimensional ion momentum distributions) of the I^{3+} fragments produced by the inner-shell ionization of 2,6-difluoroiodobenzene for delays between the UV-pump pulse and the XUV-probe pulse in the range from (a) −480 to −330 fs, i.e. for the UV pulse arriving *after* the XUV pulse, and (b) from 510 to 780 fs, i.e. for the UV pulse arriving *before* the XUV pulse. To gain better statistics, each image is integrated over approximately 1400 FEL shots after performing a centroiding routine on the single-shot images. A background image collected without the molecular beam has been subtracted. The faint spots in the middle of the image in panel (a) are background contributions that could not be fully subtracted by our subtraction routine. (c) I^{3+} fragment ion kinetic energy distributions corresponding to four different delay ranges, including the two delays shown in (a) and (b), normalized to the integrated FEL pulse energy for each delay range, and with a vertical offset with respect to each other for better visibility. The kinetic energy distributions were calculated from the radial distributions determined from the camera images using a SIMION (SIMION version 8.1 2011) simulation that connects, for each detected ion, the ion hit position on the detector to the p_x and p_y componentes of the ion momentum. Since the molecules were aligned with the iodine–carbon axis parallel to the detector plane, we assume that they have zero momentum along the z-direction, i.e. along the spectrometer axis.

intensity used in this experiment, but it can photodissociate and/or ionize the molecules into neutral and singly charged fragments, mostly leading to cleavage of the carbon–iodine bond via a resonant one-photon process (Murdock *et al* 2012). For the pump-probe experiment, we tried to adjust the intensity of the UV pulses such that most molecules were dissociated neutrally rather than being ionized by the UV pulse.

When the UV pulse arrives *after* the XUV pulse (negative time delays; figure 2(a) and black line in figure 2(c)), only intact DFIB molecules are probed by the XUV pulse, and the I^{3+} ions are produced with a high kinetic energy due to the Coulomb explosion of the molecule into several charged fragments. However, when the UV pulse arrives *before* the XUV pulse (positive time delays; figure 2(b) and blue, green, and red lines in figure 2(c)), some of the molecules have already been dissociated by the UV pulse when the XUV photons are absorbed. The kinetic energy of the corresponding I^{3+} ions is therefore strongly dependent on the delay and thus on the momentary distance between the iodine atom and the rest of the molecule. In particular, there are two low-kinetic-energy contributions, marked (II) and (III) in figure 2(c), which correspond to the strong central features in the I^{3+} ion image in figure 2(b), and which are attributed to the presence of UV-dissociated molecules. The high-kinetic-energy contribution (I) stems from intact molecules that have not been photodissociated by the UV pulse.

We have observed similar low-energy contributions in pump-probe experiments studying both the IR- and UV-induced photodissociation of CH_3I molecules and refer to our previous work (Erk *et al* 2014, Boll *et al* 2016) as well as to a forthcoming publication (Amini *et al* 2017) for a detailed discussion of their origin. Briefly, contribution (II) arises when the UV pulse dissociates the molecule by cleaving the carbon–iodine bond, and the XUV pulse then post-ionizes both fragments, leading to an increase of their kinetic energy due to the Coulomb repulsion between the charged fragments. This additional 'Coulomb energy' depends on the distance of the fragments at the time when the charge is created and thus on the delay between the UV and XUV pulses. Therefore, the kinetic energy of contribution (II) changes as a function of pump-probe delay, asymptotically approaching the kinetic energy release of the UV-induced dissociation for very long delays between the UV and the XUV pulses.

Contribution (III), on the other hand, arises when the UV pulse dissociates the molecule and the subsequent XUV pulse ionizes the iodine fragment only. If the co-fragment is neutral, this does *not* increase the fragment kinetic energy since there is no Coulomb repulsion between the iodine ion and the neutral co-fragment. The kinetic energy of contribution (III) thus stays constant for all time delays. However, at very small delays, and thus very small internuclear distances between the iodine fragment and the rest of the molecule, the co-fragment

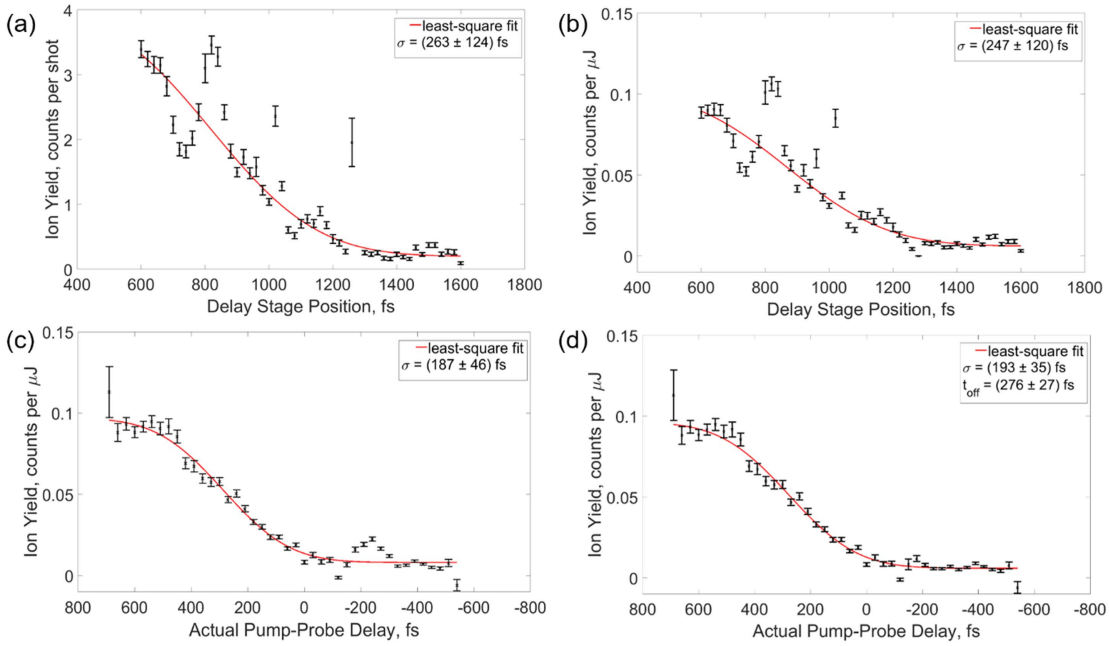

Figure 3. Yield of the low kinetic-energy contribution of the I^{3+} ions, marked as (III) in figure 2(c), as a function of the pump-probe delay. Negative delays correspond to the XUV pulse arriving before the UV pulse, positive delays to the XUV pulse arriving after the UV pulse. (a) Raw ion yield as measured during the experiment without any further corrections. (b) Same as (a) but normalized on the integrated FEL pulse energy for each delay step. (c) Same as (b) but, in addition, with the single-shot images resorted into new delay bins using the BAM data. (d) Same as (c) but after removing some shots based on the streak camera signal (see text). The red lines show the result of a least-squares fit as described in the text.

cannot remain neutral in the proximity of a highly charged iodine fragment due to charge transfer between the two moieties (Erk *et al* 2014, Boll *et al* 2016). The yield of contribution (III) therefore does not increase right at zero pump-probe delay but a few hundred femtoseconds later when the distance between the iodine fragment and the rest of the molecule has reached a critical distance beyond which charge transfer can no longer occur.

3.2. Jitter correction and further data processing

In this section, we describe the data analysis steps that are necessary to account for the FEL pulse energy fluctuations and to correct for the arrival-time jitter between the UV-pump and the FEL-probe pulses in order to obtain a data set with the highest possible temporal resolution. During the experiment, the pump-probe scans were performed by moving the delay stage in steps of 20 fs and recording 500 single-shot electron and ion images at each delay. In the post-analysis, each image was processed by a centroiding routine to identify individual ion hits, the centroided images for one delay position were then summed up, and the kinetic energy spectrum as shown in figure 2 was extracted. For the further discussion, we will concentrate on the kinetic-energy contribution marked (III) in figure 2(c) and plot its yield as a function of the pump-probe delay. Figure 3(a) shows the integrated yield of contribution (III) as measured during the experiment and without any further corrections. The plot shows an overall decrease of the signal as a function of pump-probe delay with several oscillatory features as well as individual 'outliers'. Note that compared to the standard for pump-probe experiments, the delay-dependent yields are plotted 'backwards', i.e. with the (UV-) pump-pulse arriving *earlier* than the probe pulse on the left-hand side of the plots and *later* than the probe pulse on the right-hand side of the plots. We chose this unconventional direction since it reflects the way the experiment was performed and make it easier, in the following, to link some of the observations to the actual chronology of the experiment.

The ion count rate directly depends on the FEL pulse energy, which fluctuates considerably, as shown in figure 4(a), due to the stochastic nature of the SASE process generating the XUV-FEL pulse. Therefore, it is necessary to normalize the ion yield on the single-shot FEL pulse energy. Assuming a linear dependence between the count rate and the FEL pulse energy, which we empirically found to be a sufficiently good approximation for I^{3+} in this data set, we divide the integrated count rate for each delay position by the integrated pulse energy of all FEL shots at the corresponding delay position, shown in figure 4(b), and thus obtain the normalized, delay-dependent I^{3+} ion yield displayed in figure 3(b).

Next, we correct for the arrival-time jitter and drifts in the relative timing between the pump-probe laser and the FEL, which is recorded by the BAM. Note that the BAM does *not* measure directly the arrival-time jitter between the pump-probe laser and the XUV FEL pulses, which is the actual quantity of interest, but rather the

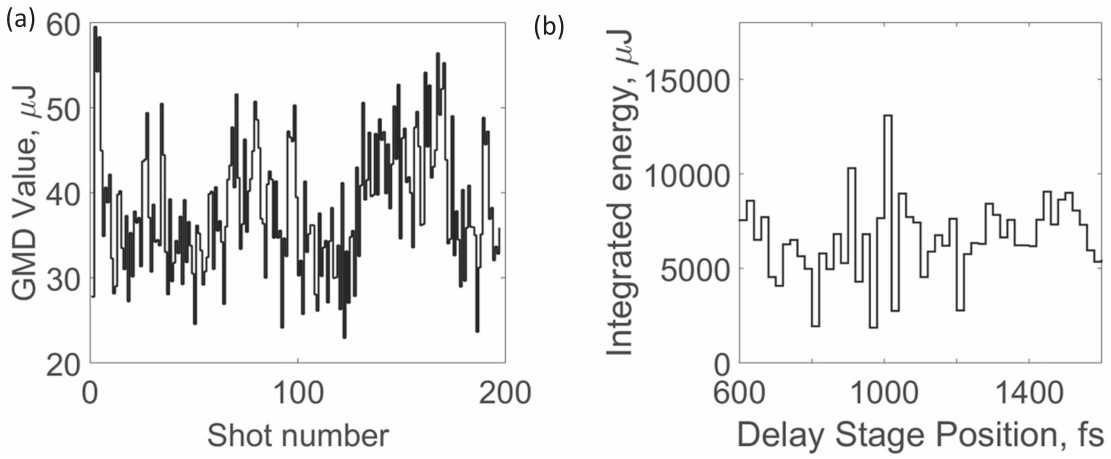

Figure 4. (a) Shot-to-shot XUV pulse energy as measured by the GMD for the first 200 shots of the delay scan. (b) Integrated XUV pulse energy for each delay stage position.

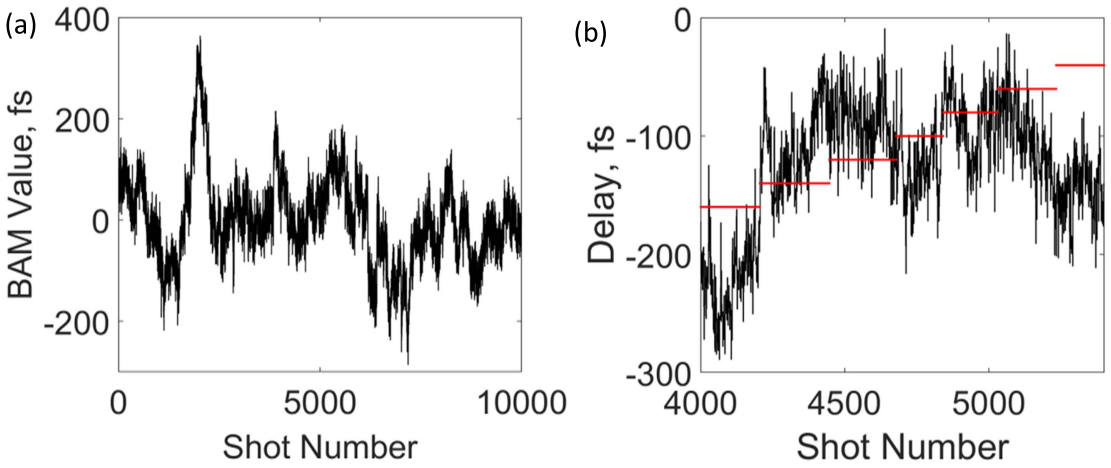

Figure 5. (a) Shot-by-shot bunch arrival-time monitor (BAM) data for all FEL shots recorded during the delay scan. (b) BAM-corrected delay (black line) compared to the nominally set delay value (red lines) for seven exemplary delay steps in the middle of the delay scan.

arrival-time jitter of the electron bunch with respect to the MLO, which should, however, be closely related, as long as all other feedback and synchronization systems are working properly (Schulz *et al* 2015). Figure 5(a) shows the BAM values for each FEL shot that were recorded during the pump-probe scan. The values shown here are measured by the BAM '4DBC3', which is located behind the last compressor chicane in the accelerator and thus shows the total energy-dependent arrival-time jitter accumulated by the electron bunch. The other BAM units are installed further upstream in the accelerator and thus only measure the jitter that has been accumulated up to that point but are used in the feedback loop mentioned in section 2.

The BAM trace in figure 5(a) shows systematic drifts in the arrival time on the order of several hundred femtoseconds as well as random shot-by-shot fluctuations that can reach up to 150 fs difference between two consecutive shots and that have an overall variance of 90 fs (rms). By including these BAM values in the analysis, we can re-calculate the actual pump-probe delay for each shot and then resort the corresponding data into new delay bins based on the BAM-corrected delay values. Figure 5(b) shows exemplarily for a given delay range how much the BAM-corrected delay (black) can deviate from the nominally set delay value (red), while figure 3(c) shows the normalized, delay-dependent I^{3+} ion yield after resorting the images using the BAM-corrected delay values. Clearly, most of the oscillations and 'outliers' in the data have now disappeared, emphasizing that they were merely artifacts caused by drifts and jitter in the arrival time of the FEL pulses. Nevertheless, the delay range between −200 and −400 fs still shows some unexpected structure. The origin of this structure is clarified when inspecting the streak camera values recorded during the delay scan, which are plotted in figure 6. At a certain time during the scan, around shot 6300 (corresponding to delays in the range −200 to −400 fs), there is a sudden jump in the streak camera values, which means that the actual pump-probe delay temporarily jumped by several

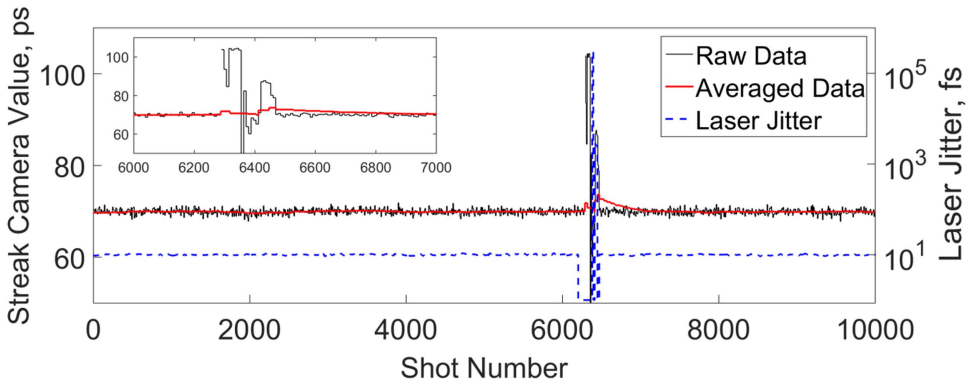

Figure 6. Raw and averaged streak camera values for the time period covered by the delay scan of interest. A simultaneous measurement of the laser lock jitter between the pump-probe laser and the master laser oscillator, as determined from the optical cross-correlator, shows that the sudden jump that occurred shortly after shot number 6000 (see zoom-in) was due to a temporary failure of the laser synchronization system.

tens of picoseconds. After further inspection of the machine data, e.g. the value of the laser jitter, which is also recorded in the DAQ system and which we also plotted in figure 6, we can attribute this jump to a short-term instability in the pump-probe laser caused by a temporary malfunction in the laser synchronization system. Since the pump-probe delay during this period is not well defined, all shots during this period, which lasted for approximately 1 min, were taken out in the last step of the analysis, resulting in the final plot shown in figure 3(d).

To extract quantitative information about the charge transfer process, which occurs on a time scale similar to the temporal resolution of the experiment, we have fitted a Gaussian cumulative distribution function

$$\mathrm{f}(x) = a + b\ \mathrm{erf}\left(\frac{x - t_{\mathrm{off}}}{\sigma}\right)$$

to the data in figure 3. Here, a and b are the baseline and the amplitude, respectively, erf is the Gauss error function, t_{off} is the center position of the step function, and σ is the temporal width of the step function, which is broadened by the temporal resolution and/or the time constant of the process. In a classical charge-transfer model, t_{off} is the time it takes the dissociating fragments to reach the critical distance for charge transfer (Erk *et al* 2014, Boll *et al* 2016). From the least-squares fit, shown as a red line in figure 3(d), we find a temporal offset of 276 fs and a width of 193 fs. Given the XUV and UV pulse durations and other factors limiting the temporal resolution of the experiment, which is discussed in more detail below, it is clear that this width reflects a convolution of the actual time constant of the charge transfer with the temporal resolution. A deconvolution of the two contributions is hampered by the fact that the experimental pulse durations, especially the duration of the UV pulse, are not known accurate enough. However, the value for the center position of the step function, t_{off}, can still be determined with a higher precision, which is given by the uncertainty of the least-squares fit and the uncertainty of the absolute time zero of the pump-probe experiment. Using the values for the total kinetic energy release for UV-induced neutral dissociation, which are 0.71 eV and 1.15 eV, depending on the dissociation channel (Murdock *et al* 2012), and assuming that this energy is immediately transformed into kinetic energy upon dissociation, the temporal offset corresponds to a critical distance of 6.3 Å and 7.9 Å, respectively, above which charge transfer between the two fragments is no longer possible within the classical model (Erk *et al* 2014, Boll *et al* 2016). We will present a more systematic study of the charge transfer process in DFIB and its dependence on the charge state of the iodine fragments in a separate publication (Amini *et al* 2017). In the following, we therefore concentrate on discussing the improvement of the temporal resolution by sorting the data according to the BAM information. The qualitative improvement of the data due to our analysis procedure is quite evident when comparing figures 3(a) and (d). Moreover, the fits in figure 3 also allow to quantify this improvement by showing a decrease of the width from 263 fs in the uncorrected data in figure 3(a) to 193 fs in the final data shown in figure 3(d). The uncertainty of the fits also decreasing drastically.

In order to quantify the improvement of the overall timing precision due to sorting according to the BAM data, we discuss, in the following, the contribution of all possible jitter sources. The major contribution stems from the jitter of the electron bunch with respect to the optical reference (σ_{bunch}), which was measured by the BAM to be 90 fs (rms) for this particular experimental run, as shown in figure 5(a). The jitter of the pump-probe laser oscillator to the optical reference (σ_{laser}) was measured to be 9 fs (rms), as shown in figure 6. According to previous measurements, the contribution from the MLO and its optical distribution (σ_{OptRef}) is ~1 fs (rms), and the sum of all other jitter contributions ($\sigma_{\mathrm{Residual}}$) is ~20 fs (rms) (Schulz *et al* 2015). The total jitter can thus be determined as $(\sigma_{\mathrm{tot\_jitter}})^2 = (\sigma_{\mathrm{bunch}})^2 + (\sigma_{\mathrm{laser}})^2 + (\sigma_{\mathrm{OptRef}})^2 + (\sigma_{\mathrm{Residual}})^2 = (90^2 + 9^2 + 1^2 + 20^2)\ \mathrm{fs}^2$,

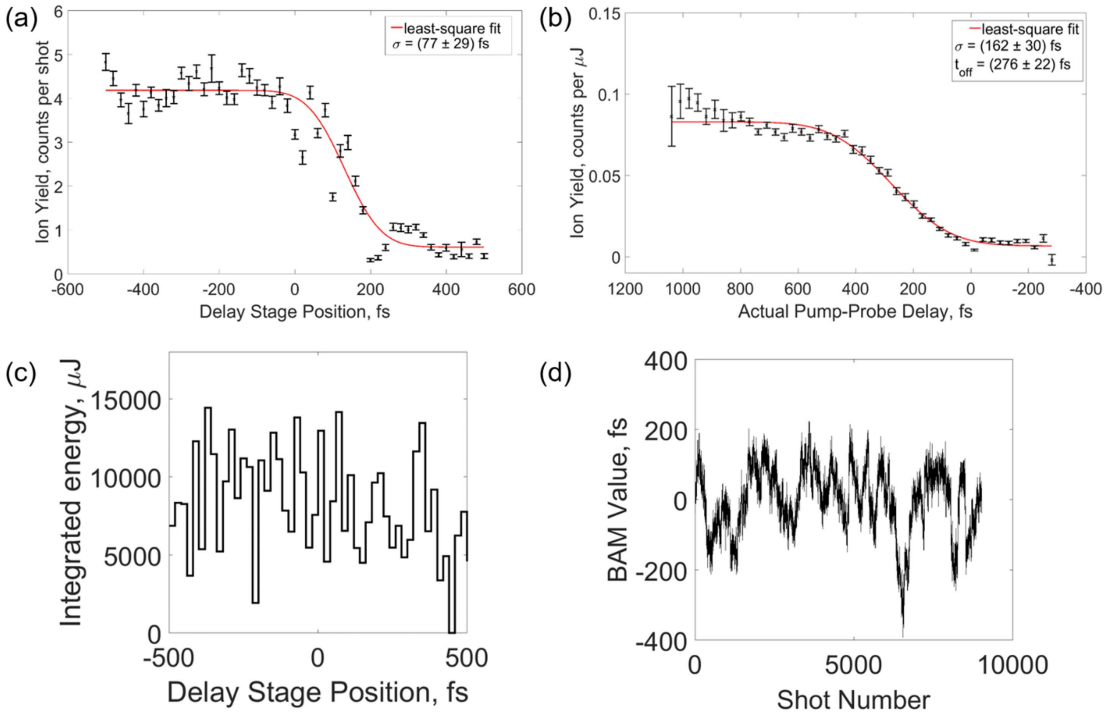

Figure 7. Same analysis as described above performed for a different scan recorded shortly after the previous data set. (a) Raw ion yield in region (III), as defined in figure 2, as measured during the experiment without any further corrections. (b) Same as (a) but normalized on the integrated FEL pulse energy for each delay step and with the single-shot images resorted into new delay bins using the BAM data. (c) Integrated XUV pulse energy for each delay stage position. (d) Shot-by-shot bunch arrival-time monitor data for all FEL shots recorded during the delay scan.

which yields a value of $\sigma_{\text{tot\_jitter}} = 93$ fs. By sorting according to the BAM data, we can correct for the jitter of the electron bunch with respect to the optical reference up to the precision of the BAM resolution, which, for the present experimental conditions, was ~15 fs (rms), thus reducing σ_{bunch} from 90 to ~15 fs. Therefore, after sorting, the remaining jitter should be $(\sigma_{\text{tot\_jitter}})^2 = (15^2 + 9^2 + 1^2 + 20^2)$ fs^2, which yields $\sigma_{\text{tot\_jitter}} = 27$ fs. Combining these values with the XUV pulse duration of ~50 fs (rms) and the UV pulse duration of ~64 fs (rms), we obtain a value for the experimental timing resolution of $\sigma_{\text{exp}} = 113$ fs *without* BAM correction and $\sigma_{\text{exp}} = 86$ fs *with* BAM correction. Given the rather long pulse durations of the XUV and UV pulses, sorting according to the BAM data therefore only results in a modest improvement of the total temporal resolution for the present experiment. However, the greater benefit, in this case, lies in the correction of systematic, non-stochastic drifts and oscillations, which can otherwise create artificially features in the experimental data, as shown in figures 3(a) and (b), that could be mistaken for real physical effects.

To further illustrate this statement and to demonstrate the sometimes unexpected results of the correction procedure, we exemplarily show, in figure 7, its application to another pump-probe scan that was recorded several hours after the data shown above. Here, the raw data in figure 7(a) seems to be less affected by sudden jumps in the arrival time, and the least-squares fit shows a quite narrow width of 77 fs. However, further analysis shows that this narrow width was actually an artifact of a strongly drifting arrival time when these delay points were recorded, such that the fully corrected data in figure 7(b) is again consistent with the results from the previous scan. This emphasizes the importance of accurate delay-time analysis, as the often non-stochastic nature of the arrival-time jitter can otherwise introduce systematic effects beyond simply broadening the experimental resolution.

Given the improved overall temporal resolution of about 200 fs (FWHM), which is no longer limited by the arrival-time jitter but only by the given pulse durations of FEL and UV pulses in this experiment, and the much improved overall quality of the data that was achieved by this systematic analysis and correction procedure, we are now able to study ultrafast effects such as the dissociation and charge transfer process in 2,6-DFIB with great precision. For a more detailed analysis and a comparison to the case of CH_3I, we refer to a separate publication (Amini *et al* 2017) that uses the tools and procedures described here.

4. Conclusions

By discussing a UV-laser-pump XUV-FEL-probe experiment studying the UV-induced photodissociation of aligned 2,6-DFIB molecules at the FLASH FEL, we have highlighted significant technical and practical improvements for femtosecond time-resolved pump-probe experiments that were achieved by recent upgrades of the FLASH timing (Kim 2007, Löhl *et al* 2010) and synchronization system (Schulz *et al* 2015). We demonstrated the importance of a careful post-analysis of the pump-probe data that takes into account the timing and diagnostics data provided by the FLASH facility. In particular, sorting of the single-shot data on the electron bunch arrival-time information obtained from the FLASH BAM significantly enhances the resolution and the overall quality of the pump-probe scans. It is also essential to identify artifacts resulting from sudden drifts or jumps in the arrival time. For the XUV and NIR/UV pulse durations that are currently available at FLASH, sorting on the BAM data corrects the relative arrival-time jitter between the FEL pulses and the pump-probe laser pulses to a level that is negligible for the total temporal resolution of the experiment, which was, in the present case, limited by the pulse durations of the FEL and the UV pulses. This confirms that the new synchronization combined with the BAM measurements allow performing NIR/UV-pump XUV-probe experiments with a high temporal resolution without additional x-ray/optical cross-correlation measurements, as long as the FEL and laser pulse durations and/or the time constants of the dynamics of interest are longer than the remaining jitter, which was on the order of 30 fs in the present experiment. However, if the pulse durations of the FEL and, especially, the optical laser were reduced significantly, limitations in the accuracy of the BAM measurements combined with other remaining jitter sources require other schemes for arrival-time measurements, such as dedicated timing tools that directly measure the arrival-time between the XUV and optical laser pulses by a cross-correlation technique. Alternatively, new schemes for timing stabilization (Şafak *et al* 2015) or new algorithms for jitter correction (Fung *et al* 2016) may be able to further reduce the jitter to a few-femtosecond level.

In addition to these technical aspects, our study has shown that the distance-dependent intramolecular charge transfer process, which we have recently studied in dissociating CH_3I and CH_3F molecules after inner-shell ionization with soft x-rays (Erk *et al* 2014, Boll *et al* 2016), also occurs in dissociating halogenated benzene compounds, as demonstrated here in the case of 2,6-DFIB. While a quantitative analysis is essentially not possible in the raw data because of the timing artifacts discussed above, we have demonstrated that the shot-by-shot analysis procedure based on the BAM allows to extract the critical internuclear distance above which charge transfer is no longer possible. A more detailed analysis of the UV-induced dissociation and charge transfer process in 2,6-DFIB and a comparison to the case of CH_3I is beyond the scope of this paper and will be the subject of a separate, forthcoming publication (Amini *et al* 2017).

5. Acknowledgments

We gratefully acknowledge the work of the scientific and technical team at FLASH, who have made these experiments possible. We also acknowledge the Max Planck Society for funding the development of the CAMP instrument within the ASG at CFEL. In addition, the installation of CAMP at FLASH was partially funded by BMBF grant 05K10KT2. NB, AR, and DR acknowledge support from the Chemical Sciences, Geosciences, and Biosciences Division, Office of Basic Energy Sciences, Office of Science, US Department of Energy, Grant No. DE-FG02-86ER13491 (Kansas group) and DE-SC0012376 (U Conn group). DR, ES, RB, CB, and BE were also supported by the Helmholtz Gemeinschaft through the Helmholtz Young Investigator Program. The CFEL group was, in addition to DESY, supported by Helmholtz Networking and Initiative Funds, by the excellence cluster 'The Hamburg Center for Ultrafast Imaging—Structure, Dynamics and Control of Matter at the Atomic Scale' of the Deutsche Forschungsgemeinschaft (CUI, DFG-EXC1074), and by the Helmholtz Virtual Institute 419 'Dynamic Pathways in Multidimensional Landscapes'. JK, PJ, HS, and DR also thank the EU for support via the MEDEA project within the Horizon 2020 research and innovation programme under the Marie Skłodowska-Curie grant agreement No 641789. S Te is grateful for support through the Deutsche Forschungsgemeinschaft, project B03/SFB755 and project C02/SFB1073. KA, AL, M Bu, and M Br gratefully acknowledge support from the EPSRC Programme Grant EP/L005913/1. PJ acknowledges support from the Swedish Research Council and the Swedish Foundation for Strategic Research. AR is grateful for support through the Deutsche Forschungsgemeinschaft project RO 4577/1-1.

References

Ablikim U *et al* 2017 *Phys. Chem. Chem. Phys.* submitted
Ackermann W *et al* 2007 *Nat. Photon.* **1** 336
Allaria E *et al* 2012 *Nat. Photon.* **6** 699–704

Amini K, Savelyev E et al 2017 in preparation
Aquila A et al 2012 Opt. Express 20 2706–16
Azima A et al 2009 Appl. Phys. Lett. 94 144102
Barends T R M et al 2015 Science 350 445
Behrens C, Gerasimova N, Gerth C, Schmidt B, Schneidmiller E A, Serkez S, Wesch S and Yurkov M V 2012 Phys. Rev. ST Accel. Beams 15 069902
Beye M et al 2012 Appl. Phys. Lett. 100 121108
Biasin E et al 2016 Phys. Rev. Lett. 117 013002
Bionta M R et al 2011 Opt. Express 19 21855
Bionta M R et al 2014 Rev. Sci. Instrum. 85 083116
Boll R et al 2014 Faraday Discuss. 171 57–80
Boll R et al 2016 Struct. Dyn. 3 043207
Budarz J M, Minitti M P, Cofer-Shabica D V, Stankus B, Kirrander A, Hastings J B and Weber P M 2016 J. Phys. B: At. Mol. Opt. Phys. 49 034001
Clark J N et al 2015 Proc. Natl Acad. Sci. 112 7444
Czwalinna M K 2012 PhD Thesis Universität Hamburg
Dell'Angela M et al 2013 Science 339 6125
Drescher M, Frühling U, Krikunova M, Maltezopoulos T and Wieland M 2010 J. Phys. B: At. Mol. Opt. Phys. 43 194010
Düsterer S et al 2013 J. Phys. B: At. Mol. Opt. Phys. 46 164026
Düsterer S et al 2014 Phys. Rev. ST Accel. Beams 17 120702
Eckert S et al 2015 Appl. Phys. Lett. 106 061104
Emma P et al 2010 Nat. Photon. 4 641
Erk B et al 2014 Science 345 288
Fang L, Osipov T, Murphy B F, Rudenko A, Rolles D, Petrovic V S, Bostedt C, Bozek J D, Bucksbaum P H and Berrah N 2014 J. Phys. B: At. Mol. Opt. Phys. 47 124006
Feldhaus J 2010 J. Phys. B: At. Mol. Opt. Phys. 43 194002
Ferguson K R et al 2016 Sci. Adv. 2 1500837
Filsinger F, Küpper J, Meijer G, Hansen J L, Maurer J, Nielsen J H, Holmegaard L and Stapelfeldt H 2009 Angew. Chem., Int. Ed. 47 6900–2
Flückiger L et al 2016 New J. Phys. 18 043017
Fung R, Hanna A M, Vendrell O, Ramakrishna S, Seidemann T, Santra R and Ourmazd A 2016 Nature 532 417–75
Gahl C et al 2008 Nat. Photon. 2 165–9
Gleason A E et al 2015 Nat. Commun. 6 8191
Glownia J M et al 2010 Opt. Express 18 017620
Gorkhover T et al 2016 Nat. Photon. 10 93–7
Grguraš I et al 2012 Nat. Photon. 6 852–7
Hallmann J et al 2010 J. Phys. B: At. Mol. Opt. Phys. 43 194009–16
Harmand M et al 2013 Nat. Photon. 7 215–8
Holmegaard L, Nielsen J H, Nevo I, Stapelfeldt H, Filsinger F, Küpper J and Meijer G 2009 Phys. Rev. Lett. 102 023001
Ishikawa T et al 2012 Nat. Photon. 6 540–4
Jiang Y H et al 2010a Phys. Rev. Lett. 105 263002
Jiang Y H et al 2010b Phys. Rev. A 82 041403(R)
Jiang Y H et al 2010c Phys. Rev. A 81 051402(R)
Jiang Y H et al 2013 J. Phys. B: At. Mol. Opt. Phys. 46 164027
Johnsson P et al 2009 J. Phys. B: At. Mol. Opt. Phys. 42 134017
Kim J 2007 Opt. Express 32 1044–6
Krikunova M, Maltezopoulos T, Wessels P, Schlie M, Azima A, Gaumnitz T, Gebert T, Wieland M and Drescher M 2012a Phys. Rev. A 86 043430
Krikunova M, Maltezopoulos T, Wessels P, Schlie M, Azima A, Wieland M and Drescher M 2011 J. Chem. Phys. 134 024313
Krikunova M et al 2009 New J. Phys. 11 123019
Krikunova M et al 2012b J. Phys. B: At. Mol. Opt. Phys. 45 105101
Küpper J et al 2014 Phys. Rev. Lett. 112 0830002
Larsen J J, Hald K, Bjerre N and Stapelfeldt H 2000 Phys. Rev. Lett. 85 2470
Lehmann C S et al 2016 Phys. Rev. A 94 013426
Liekhus-Schmaltz C E 2015 Nat. Commun. 6 8199
Löhl F et al 2010 Phys. Rev. Lett. 104 144801
Maltezopoulos T et al 2008 New J. Phys. 10 033026
McFarland B K et al 2014 Nat. Commun. 5 4235
Meyer M et al 2006 Phys. Rev. A 74 011401
Meyer M et al 2008 Phys. Rev. Lett. 101 193002
Meyer M et al 2010 J. Electron Spectrosc. Relat. Phenom. 181 111–5
Minitti M P et al 2015 Phys. Rev. Lett. 114 255501
Murdock D et al 2012 J. Chem. Phys. 136 124313
Nevo I et al 2009 Phys. Chem. Chem. Phys. 11 9912
Öström H et al 2015 Science 347 978–82
Pande K et al 2016 Science 352 725–9
Picon A et al 2016 Nat. Commun. 7 11652
Petrovic V S et al 2012 Phys. Rev. Lett. 108 253006
Radcliffe P et al 2007 Nucl. Instrum. Methods Phys. Res. A 583 516–25
Rajkovic I et al 2010 Phys. Rev. Lett. 104 125503
Redlin H, Al-Shemmary A, Azima A, Stojanovic N, Tavella F, Will I and Düsterer S 2011 Nucl. Instrum. Methods Phys. Res. A 635 S88–93
Ren X, Makhija V and Kumarappan V 2014 Phys. Rev. Lett. 112 173602
Rettig L et al 2016 Phys. Rev. Lett. 116 257202
Riedel R et al 2013 Nat. Commun. 4 1731

Rolles D *et al* 2014 *J. Phys. B: At. Mol. Opt. Phys.* **47** 124035
Rouzée A *et al* 2013 *J. Phys. B: At. Mol. Opt. Phys.* **46** 164029
Rudenko A and Rolles D 2015 *J. Electron Spectrosc. Relat. Phenom.* **204** 228–36
Şafak K, Xin M, Callahan P T, Peng M Y and Kärtner F X 2015 *Struct. Dyn.* **2** 041715
Schnorr K *et al* 2013 *Phys. Rev. Lett.* **111** 093402
Schnorr K *et al* 2014a *Phys. Rev. Lett.* **113** 073001
Schnorr K *et al* 2014b *Faraday Discuss.* **171** 41
Schnorr K *et al* 2015 *J. Electron Spectrosc. Relat. Phenom.* **204** 245–56
Schorb S *et al* 2012 *Appl. Phys. Lett.* **100** 121107
Schulz S *et al* 2015 *Nat. Commun.* **6** 5938
Shintake T *et al* 2008 *Nat. Photon.* **2** 555–9
Siefermann K R *et al* 2014 *J. Phys. Chem. Lett.* **5** 2753
SIMION version 8.1 2011 http://simion.com/
Stapelfeldt H and Seideman T 2003 *Rev. Mod. Phys.* **75** 543
Stern S *et al* 2014 *Faraday Discuss.* **171** 393–418
Strüder L *et al* 2010 *Nucl. Instr. Meth. Phys. Res.* A **614** 483–96
Tenboer J *et al* 2014 *Science* **346** 1242
Tiedtke K *et al* 2008 *J. Appl. Phys.* **103** 094511
Viftrup S S, Kumarappan V, Trippel S and Stapelfeldt H 2007 *Phys. Rev. Lett.* **99** 143602
Wernet P *et al* 2015 *Nature* **520** 78–81
Yeh J J 1993 *Atomic Calculation of Photoionization Cross-Sections and Asymmetry Parameters* (Langhorne, PE: Gordon and Breach)